Generation mechanism of a dipole field by a magnetohydrodynamic dynamo

Akira Kageyama and Tetsuya Sato
Theory and Computer Simulation Center, National Institute for Fusion Science, Nagoya 464-01, Japan
(Received 12 September 1996)

Computer simulation of a magnetohydrodynamic dynamo in a rotating spherical shell is performed. A strong magnetic field is generated by thermal convection motion of an electrically conducting fluid. The generated magnetic field has a well-organized structure. The field is expanded by the spherical harmonics Y_ℓ^m. The leading moment is the dipole ($\ell=1,m=0$) which is 1.3 times larger than the second moment, octapole ($\ell=3,m=0$). These two moments occupy more than half of the total power of the magnetic field. Structure and the generation mechanism of the magnetic field are examined in detail. It is found that the well-known α-ω dynamo scenario gives a good explanation of the whole dynamo cycle. [S0556-2821(97)06503-X]

PACS number(s): 52.30.−q, 52.65.Kj, 95.30.Qd, 97.10.Ld

I. INTRODUCTION

In this paper, we investigate the magnetohydrodynamic (MHD) dynamo by thermal convection motion of plasma in the geometry of a rotating spherical shell, such as a stellar convection zone. The self-consistent computer simulation of the MHD dynamo has been performed by many authors [1–13]. Our model would be appropriate for solar-type stars, but our present interest is in the understanding of general MHD dynamo physics, rather than a direct comparison with a special star. Many dynamo studies focus on the so-called α effect [14–16]. This is reasonable since an essential process of the field generation is extracted in the α effect. It should be stressed, however, that the studies of the α effect are physically inconsistent unless it is proven that the convection motion driven by thermal energy naturally has a flow pattern which produces the α effect. In this paper, time developments of thermal convection motion as well as the magnetic field are self-consistently calculated. The solved equations are the full set of the MHD equations. There is no explicit α-effect term in the induction equation. We have reported in previous papers that a strong magnetic field, whose energy becomes greater than convection energy, is generated [17], and a dominant dipole magnetic field is spontaneously generated [18]. In this paper, we present a physical mechanism of how the dipole field is generated.

II. MODEL AND METHOD

We set up a simulation model as simple as possible since our present purpose is to understand the fundamental process of the MHD dynamo. Suggested by a stellar convection zone, we consider a spherical shell geometry [see Fig. 1(a)]. The system consists of an inner spherical core that has a heat source to keep its surface ($r=r_i$) at high temperature, an outer heat absorbing spherical boundary surface ($r=r_o$) that is kept at low temperature, and an intermediate conductive fluid medium sandwiched by the two spherical boundaries ($r=r_i$ and r_o). The conductive medium is represented by the MHD equations with gravity force. The calculation is implemented on a spherical coordinate (r,ϑ,φ) grid point system with a finite difference method [17,19].

Simulations are performed in a full spherical shell region ($r_i\leqslant r\leqslant r_o, 0\leqslant\vartheta\leqslant\pi, 0\leqslant\varphi\leqslant 2\pi$). The grid numbers $(N_r,N_\vartheta,N_\varphi)$ are chosen to be (50,38,64). The boundary conditions at $r=r_i$ and r_o are such that $\mathbf{v}=0$ and $E_r=\partial E_\vartheta/\partial r=\partial E_\varphi/\partial r=0$. This means that the magnetic field has only radial components on the boundaries ($B_r\neq 0$, $B_\vartheta=B_\varphi=0$) [17,1]. This boundary condition is proper for a solar dynamo problem since it is observed that the magnetic field at the photosphere is always perpendicular to the surface [1]. This boundary condition guarantees the poynting flux $\mathbf{E}\times\mathbf{B}$ through the boundary to be zero, since the vector $\mathbf{E}\times\mathbf{B}$ has no radial component. Therefore, we can definitely say that a strong magnetic field in the spherical shell obtained at the end of this simulation is a result of an MHD dynamo process, not an artificial or numerical inflow of magnetic energy through the boundaries.

The parameters used in this simulation are as follows: $r_i=0.3$, $r_o=1.0$, $R=1\times10^4$, $\eta=2.7\times10^{-4}$, $T=5.88\times10^6$, $\mathrm{Pr}=1$, $\mathrm{Pr}_m=10.6$, where R, η, T, Pr, Pr_m are a Rayleigh number, nondimensional resistivity normalized by $\mu_0 c_s r_o$ (c_s is sound speed), a Taylor number, a Prandtl number, and a magnetic Prandtl number, respectively. These parameters are defined as follows: $R=(g/T_o)(\beta c_p-g)(r_o-r_i)^4/[(\kappa/\rho_o)(\nu/\rho_o)]$, $T=[2\Omega(r_o-r_i)^2/\nu]^2$, $\mathrm{Pr}=\nu/\kappa$, $\mathrm{Pr}_m=\nu/\eta$, where T_o and ρ_o are temperature and mass density at the outer sphere; g=gravity acceleration, β=temperature gradient coefficient, (the initial temperature profile is given by $\beta/r+\mathrm{const.}$) c_p=specific heat with constant pressure, κ=thermal conductivity, ν=viscosity, and Ω=rotation angular velocity of the spherical shell. Although the purpose of this paper is not to simulate the sun or other specific star, it would be helpful to show various values adopted in this simulation in dimensional form. If we take the outer radius r_o, mass density $\rho(r_o)$, and temperature $T(r_o)$ as the solar values [20] [$r_o=6.7\times10^8$(m), $\rho(r_o)=8\times10^{-5}$ kg m^{-3}, and $T(r_o)=6.6\times10^3$ K], other dimensional values can be calculated as, for example, heat flux$=1.1\times10^5$ J/s m^2, gravity acceleration$=4.1$ m/s^2, viscosity $\nu=1.1\times10^6$ kg/m s, thermal conductivity $\kappa=1.4\times10^{10}$ W/mK, resistivity $\eta=1.7\times10^3\Omega$m. Some of these values are quite different from those of the sun. Especially, the last three dissipation coefficients are apparently too high for a high temperature plasma. This means that we

simulate an MHD dynamo in a system of strong dissipation limit.

Time development of the difference MHD equations are calculated by the fourth-order Runge-Kutta method [21]. Time is normalized by sound crossing time ($=r_o/c_s$). In this normalization, the thermal diffusion time τ_{th}, viscous diffusion time τ_{vis} and resistive diffusion time τ_{res} are given, respectively, by $\tau_{th}=\tau_{vis}=240$ and $\tau_{res}=3700$. The simulation is made until $t=5500$, that is about 23 τ_{th} (τ_{vis}) or 1.5 τ_{res}. The sphere rotates about 6130 times in this period. The turnover time of the convection motion is roughly ten times of the rotation period of the sphere.

III. RESULTS

A. Structure of convection motion

The initial condition is given by a hydrostatic and thermal equilibrium state with no magnetic field. A thermal convection instability, with no magnetic field, grows when a weak random noise is superimposed upon the initial temperature profile. Thermal convection in rotating spherical shells has been investigated by theory [22,23] and numerical simulation [24–27,19,28]. In our calculation, the convection reaches a saturated state at $t=150$. The saturated convection motion is nonturbulent and has almost no temporal fluctuation. The convection pattern slowly drifts westward. Well-organized anticyclonic and cyclonic columnar cells, or, anticyclonic and cyclonic convection columns, whose axes are parallel to the rotation axis (z axis), are formed in pairs (side by side) and encircle the rotation axis [see Fig. 1(b)]. The formation of the straight convection columns are due to the Taylor-Proudman theorem [29]. It is known that there is another constraint of an MHD fluid in a rotating system which was found by Taylor [30]. However, Taylor's constraint is not satisfied in our simulation since the necessary condition for this constraint (negligibly small viscosity and very slow flow) is not satisfied in our case.

The fluid in a cyclonic (anticyclonic) column rotates in the same (opposite) direction as the rotation of the spherical shell. The columns have negative (positive) helicity, $\mathbf{v}\cdot\omega$, in the northern (southern) hemisphere due to the axial, or z-, flow component in each column which is directed toward (away from) the equator in the cyclonic (anticyclonic) columns. This axial flow induces horizontally converging, or sucking, flow near the outer boundary at both (northern and southern) ends of the cyclonic columns. This horizontal converging flow plays an important role in the dipole field generation which will be explained later on. Effects of compressibility on the convection dynamics are weak in this calculation since the maximum speed of the convection velocity is about 10% of the sound velocity.

B. Magnetic field generation

After the convection motion has reached the saturated state (at $t=256$), we superimpose a weak seed of a random magnetic field. The seed field is given by the curl of the following vector potential having only the radial component; $A_r=\sin[(r-r_i)\pi/(r_o-r_i)]\times F(\vartheta,\varphi)$, where the function F is a random field with small amplitude: The value of F on each grid point is determined by a random number generator between 0 and 0.001. The amplitude of the initial magnetic energy induced from this vector potential is only 1.61×10^{-3} of the convection kinetic energy. Although the initial magnetic field has a complicated structure, we get a simple magnetic field structure at the end.

After a short while, the magnetic energy starts growing exponentially. The magnetic energy grows beyond the kinetic energy at about $t=4000$ and saturates at an energy level about two times larger than the kinetic energy in the present case. Both energies have no appreciable temporal variations in the final state. The convection motion in the final state is nonturbulent and keeps its well-organized structure. One of the interesting findings of this simulation is that in spite of the existence of such a strong magnetic field, the columnar structure of the convection motion is not destroyed. This can be explained by the fact that the generated magnetic field is nearly force free ($\mathbf{J}\times\mathbf{B}\sim\mathbf{0}$) in the most part.

C. Structure of magnetic field

In order to understand the generation mechanism of the magnetic field, we examine in detail the magnetic field structure in the shell at $t=3400$ when the magnetic energy is exponentially growing. It is found that dividing the magnetic field into toroidal and poloidal parts helps understanding the field structure. The blue lines in Fig. 2 show the toroidal field lines. Figures 2(a) to 2(d) show four different views. There are 12 field lines in Fig. 2 (six in each hemisphere) which are all traced for a length of 17.14 (in the unit of r_o) though the field lines can be traced much more. The gray transparent barlike objects are isosurfaces of positive z component of vorticity ω_z which stands for cyclonic convection columns. There is a strong toroidal magnetic fluxes in each hemisphere. The polarity of these toroidal fluxes is antisymmetric about the equator; westward in the northern hemisphere and eastward in the southern hemisphere. An interesting feature of the toroidal field is that the shape of the lines viewed from north [Fig. 2(a)] is like a flower with six petals. It will be shown that this characteristic shape of the lines is a key to understand the generation mechanism of the magnetic field.

The green and red lines in Fig. 3 show poloidal field lines in the spherical shell. All the lines are traced from the outer boundary ($r=r_o$). The starting points of the lines are chosen so that the magnetic field strength $|B|$ at the points are greater than 50% of maximum value $|B|_{max}$ on the outer boundary. In contrast to the toroidal field lines (Fig. 2), the poloidal field lines (Fig. 3) cannot be traced far, since they soon reach the spherical boundaries. The lines are colored due to the position of each line's end point. The end point of a red line is on the inner boundary. In other words, the red lines connect two points, one of which is on the outer boundary and the other on the inner boundary. On the other hand, the end point of a green line is on the outer boundary: Green lines connect two points which are both on the outer boundary. A distinct feature of Fig. 3 is that all the field lines near the outer boundary are converged in the six cyclonic columns. The convergence mechanism will be explained later on.

A spontaneously generated magnetic field on the outer boundary $B_r(r=r_o)$ is expanded by spherical harmonics

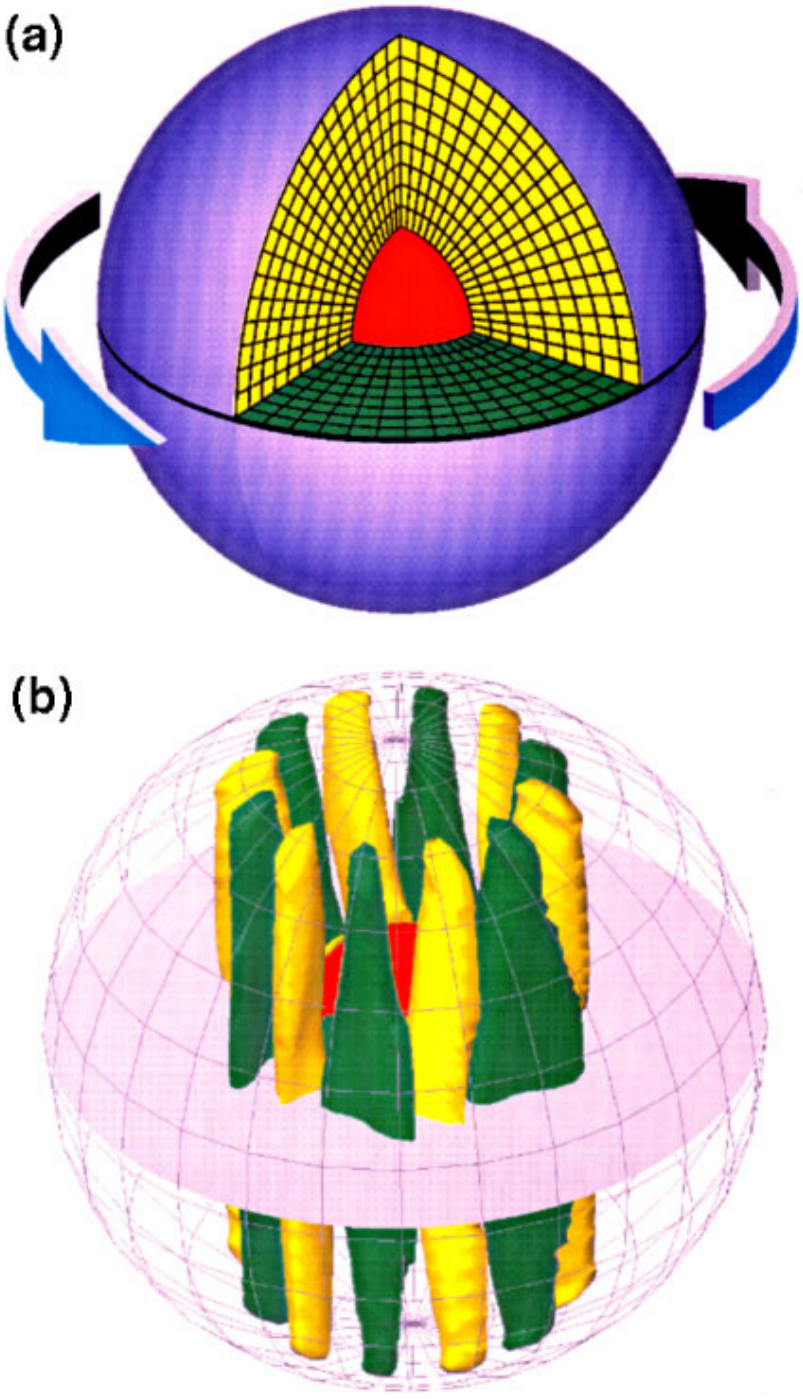

FIG. 1. (Color) Simulation model and convection cells. (a) The interior of the model is exposed by cutting a piece of the sphere. The green part represents the equatorial plane and the yellow does two meridional planes. The meshes indicated in these planes illustrate how the system is implemented on a grid point system. The number of grids shown here does not represent the actual one but is reduced for brevity. An electrically conducting fluid is sandwiched by two concentric spheres with different temperatures; hot (red) and cold (violet). The system is rotating with a constant angular velocity as shown by arrows. (b) Well-organized columnar convection cells (convection columns) obtained by the simulation with no magnetic field. These are visualized by isosurfaces of axial component of vorticity, ω_z. The cyclonic columns (green) and anticyclonic columns (yellow) appear in an alternate way to encircle the rotation axis.

$Y_\ell^m(\vartheta,\varphi)$; $B_r(r_o)=\Sigma_{\ell=1}\Sigma_{m=-\ell}^{\ell} a_\ell^m Y_\ell^m$. On comparing powers of each mode, we find that the most strongly excited mode is the dipole moment ($\ell=1,m=0$). In the final state ($t=5500$), $|a_1^0|^2=3.4\times10^{-4}$. The second moment is the octapole: $|a_3^0|^2=2.0\times10^{-4}$. The third one is a nonaxisymmetric moment ($\ell=7,m=\pm6$), $|a_7^6|^2+|a_7^{-6}|^2=1.4\times10^{-4}$. [The azimuthal mode number $|m|=6$ comes from six pairs of convection columns; see Fig. 1(b).] The quadrupole ($\ell=2,m=0$) is very weak: $|a_2^0|^2=6.8\times10^{-6}$. All these numbers stay at the same levels after the dynamo saturation. More generally, the moments with the quadrupole symmetry ($\ell+m=$even) remain at a very low amplitude compared with the moments with the dipole symmetry ($\ell+m=$odd). Here the dipole symmetry means that $B_r(\vartheta)=-B_r(\pi-\vartheta)$, while the quadrupole symmetry means that $B_r(\vartheta)=B_r(\pi-\vartheta)$.

In Fig. 4(a), azimuthally averaged poloidal magnetic components are shown by thick solid lines (yellow) and intensities of toroidal components are color plotted: Red (blue) denotes westward (eastward) toroidal field. Illustrated in Fig. 4(b) is a three-dimensional structure of magnetic field lines of the potential field at a final state ($t=5500$). Each line is colored in order to show the direction of the magnetic field (blue → green → red). It is obviously seen in Figs. 4(a) and 4(b) that the magnetic field with the dipole symmetry is strongly excited.

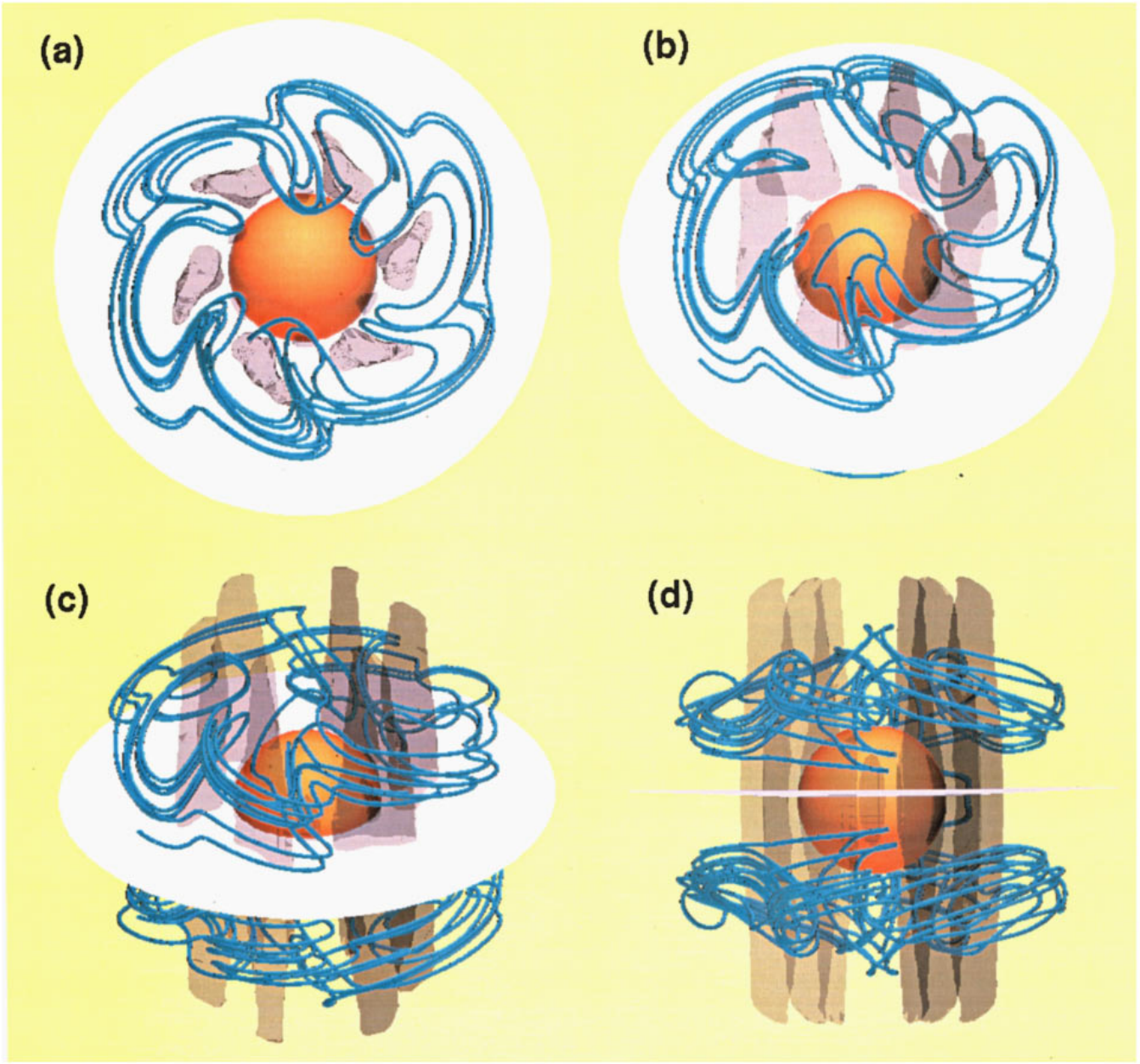

FIG. 2. (Color) Toroidal magnetic field structure. Toroidal field lines (blue) are traced at $t=3400$ when the magnetic energy is exponentially growing. The four panels (a) to (d) are views from four different angles. (a) is from the north and (d) is from the equator. The semitransparent gray barlike objects are cyclonic convection columns visualized by isosurfaces of vorticity ω_z.

D. Generation mechanism of dipole field

Let us now go on to the generation mechanism of the dipole field. We pay attention to a pair of cyclonic and anticyclonic columns in the northern hemisphere [see Fig. 5(a)]. Suppose that there is a westward toroidal magnetic field line encircling convection columns in the northern hemisphere at the middle latitude [line 1 in Fig. 5(a)]. Because of the rotating motion of each column, the field line is swallowed up in the valley of anticyclonic and cyclonic columns (cyclonic in the west, anticyclonic in the east), namely, toward the inner sphere (line 2). This stretches the field line against the field tension force ($-\mathbf{v}\cdot\mathbf{J}\times\mathbf{B}>0$; positive dynamo). Simultaneously, the axial flow, or z-component flow in the columns pulls up the sheared line and generates z-, or poloidal, component of the magnetic field (line 3). The same process takes place in the southern hemisphere, too. The generated field line configuration in the northern and southern hemispheres is deformed as shown in Fig. 5(b), since the toroidal component is antisymmetric about the equator [see the color in Fig. 4(a)]. Then, the field lines in both hemispheres reconnect with each other on the equatorial plane at points $a, a', a'', \ldots$ in Fig. 5(b). Field line reconnection leads to the formation of six poloidal field lines as shown in Fig. 5(c) since there are six pairs of cyclonic and anticyclonic convection columns.

Figure 6 shows that the above process is certainly taking place in our simulation. A magnetic field line at $t=3400$ (the same data as Figs. 2 and 3) is shown in Fig. 6. The field line is colored depending on the value of the dynamo term $-\mathbf{v}\cdot(\mathbf{J}\times\mathbf{B})$ at each point on the line. The line becomes red

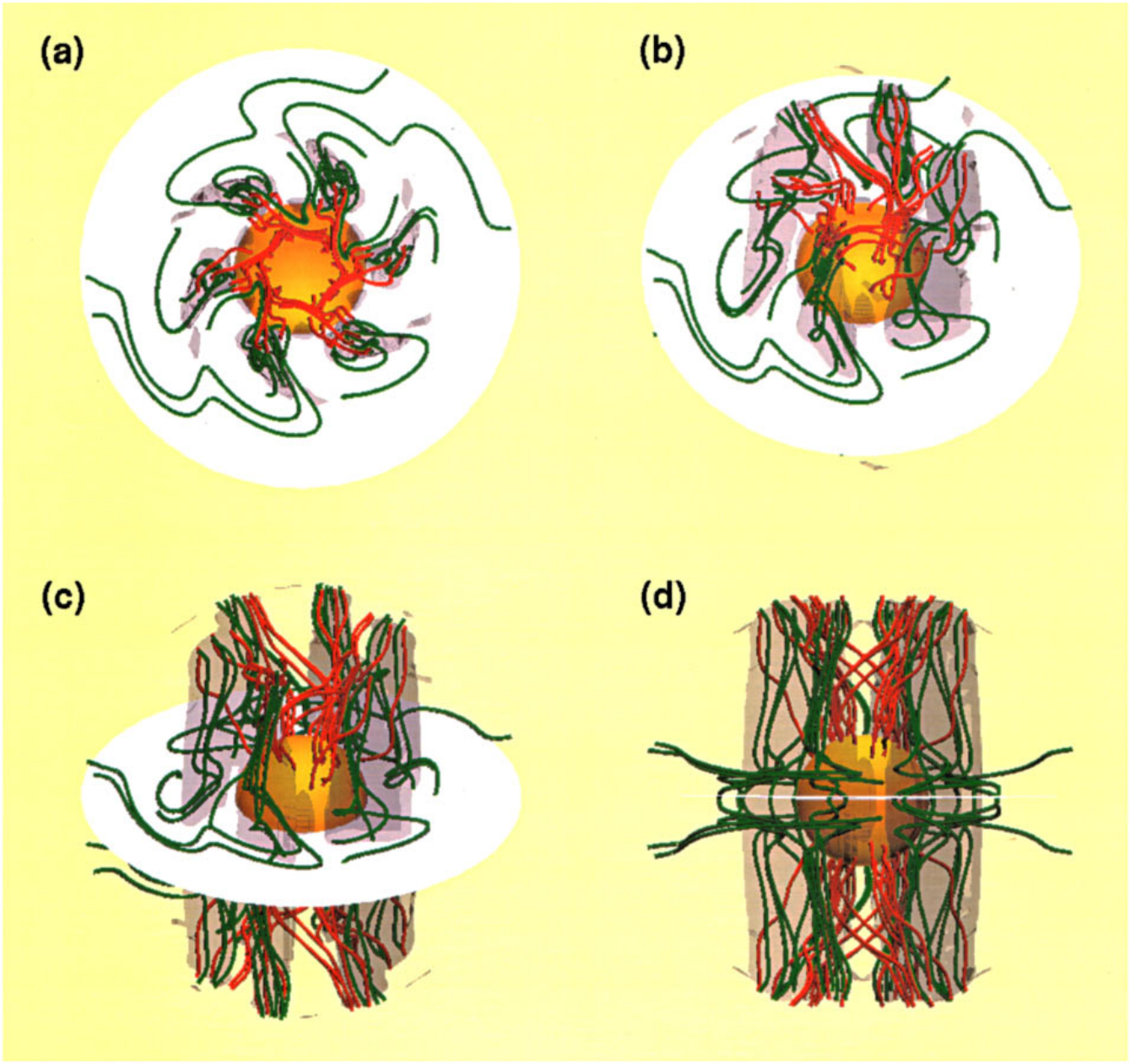

FIG. 3. (Color) Poloidal magnetic field structure. Poloidal field lines (red and green) are traced at $t=3400$ when the magnetic energy is exponentially growing. The four panels (a) to (d) are views from four different angles. (a) is from the north and (d) is from the equator. The semitransparent gray barlike objects are cyclonic convection columns visualized by isosurfaces of vorticity ω_z. All the field lines are traced from the outer spherical boundary. The lines are colored depending on the end point of each line: The red lines end at the inner boundary and the green lines end at the outer boundary.

where the term is large positive. In other words, a strong dynamo action is taking place in regions where the field line is red. The white arrows on the line stand for the strength and direction of the flow velocity at the points. Semitransparent barlike objects are convection columns visualized by isosurfaces of $\omega_z=\pm 0.6$. The blue ($\omega=0.6$) one denotes a cyclonic convection column and the pink ($\omega=-0.6$) one denotes an anticyclonic column. We can intuitively understand from Fig. 6 how the poloidal component is generated by the deformation of the field line. And the arrows indicate that the inward flows between the columns are in the opposite direction of the field line's tension force. Therefore, $-\mathbf{v}\cdot\mathbf{J}\times\mathbf{B}$ becomes positive there, which means that the magnetic energy is generated at those points. Glatzmaier and Roberts [12,13] have also shown that a dipole field is generated by the MHD convection in a rotating spherical shell. The dynamo mechanism of their simulation is quite different from ours because of a very different parameter range.

It should be noted here that the above process of the poloidal field generation can be understood as an α effect. The negative (positive) helicity in the northern (southern) hemisphere generates parallel (antiparallel) current to the toroidal magnetic field. (But note that this α effect is self-consistently induced by nonturbulent MHD convection.)

We also point out a similarity between the above explained dipole field generation process and a field-reversed

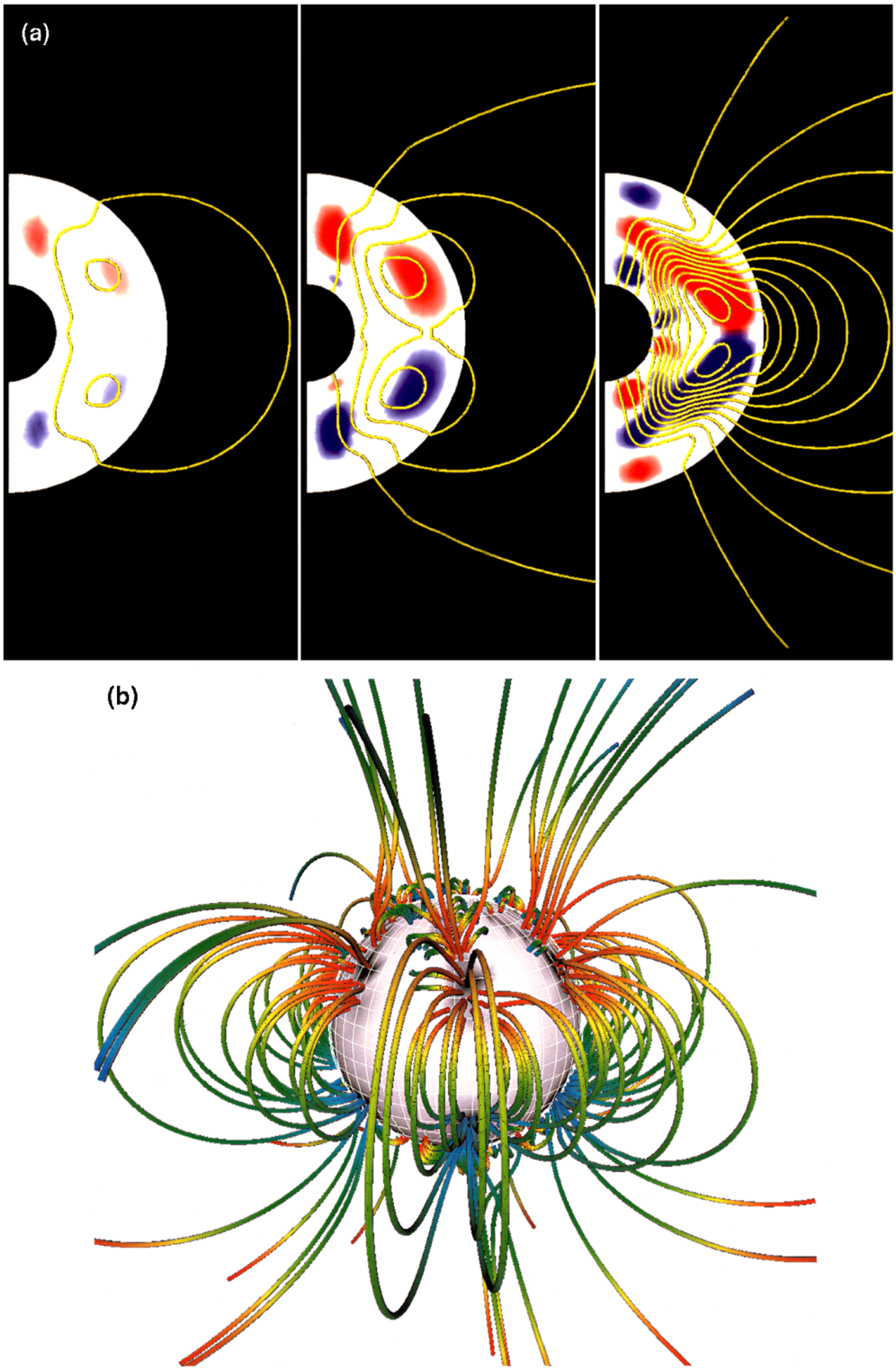

FIG. 4. (Color) Dipole field generation. (a) The three panels show three time sequential color plots of the azimuthally averaged meridional (poloidal) component of the generated magnetic field in a meridian plane (yellow). The number of lines represents the intensity of the field. The bright disclike region represents the simulation region where the innermost part is the hot temperature boundary and the outermost is the low temperature boundary. The reddish part is the color contour of the averaged westward toroidal field and the bluish is that of the eastward one. One can confirm from these color plots that the dipole-dominant field originates from the pair of the westward (northern hemisphere) and eastward (southern hemisphere) components of the toroidal field. (b) Three-dimensional view of magnetic field lines of the potential field emerged through the outer spherical boundary from the convection columns at the final state ($t=5500$). Each magnetic field line is colored in order to show the direction of the magnetic field (blue → green → red). One can clearly see that the dipole field is preferentially generated.

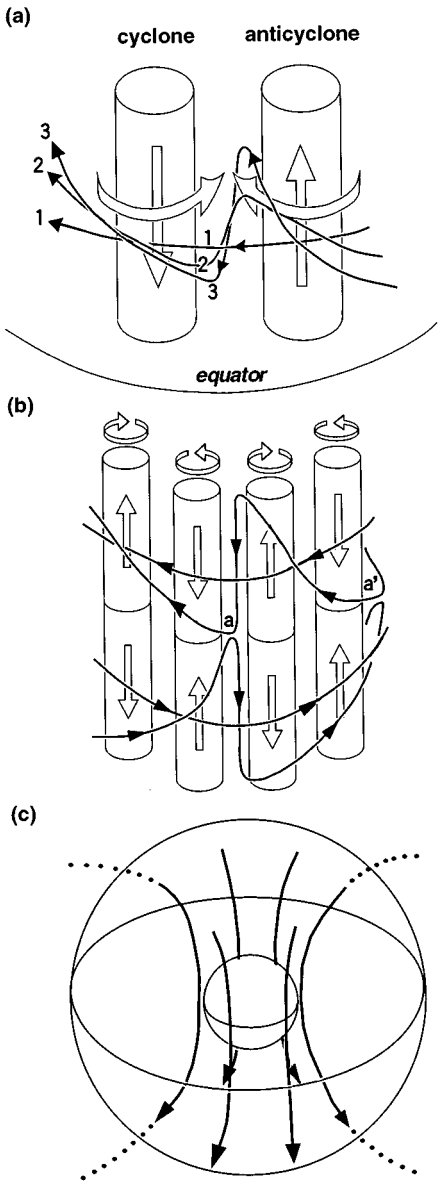

FIG. 5. Dynamo mechanism. (a) Schematic diagram of the dipole field generation mechanism. A pair of cyclonic column (west) and anticyclonic column (east) and magnetic field lines in the northern hemisphere are shown. The magnetic field line 1 encircle the convection columns. The lines are swallowed up toward the inner sphere at the boundary region between cyclonic and anticyclonic columns because of the rotating motion of the columns (denoted by white horizontal big arrows). [On the other hand, the field lines are pushed out at the anticyclonic (west)-cyclonic (east) boundary.] Axial, or z-, component flows in the columns (denoted by vertical white big arrows) shear the field line so as to generate the southward component of the magnetic field (lines 2 and 3). The field lines are strongly stretched, so that the dynamo, $-\mathbf{v}\cdot\mathbf{J}\times\mathbf{B}$ takes place at this place. (b) The poloidal field generation process from the toroidal field explained in (a) takes place in the southern hemisphere, too. Since the toroidal field in the southern hemisphere is eastward [see Fig. 4(a)], the generated poloidal lines in both hemispheres reconnect with each other on the equatorial plane at points a, a', a'', etc. (c) Six poloidal field lines are generated since there are six pairs of cyclonic and anticyclonic convection columns [see Fig. 1(b)].

configuration (FRC) formation process in plasma experiments. It is known from both laboratory [31,32] and numerical [33] experiments that when two spheromaks collide head on, they are merged together and an isolated plasma with singly connected flux surfaces is formed. The resultant field configuration is an FRC when the two spheromaks have opposite signs of the magnetic helicity. Antiparallel toroidal fields in each spheromak canceled each other after the merging and a purely poloidal field is left. The poloidal field generation observed in this dynamo simulation is similar to this FRC formation by merging of two spheromaks. The two spheromaks correspond to two toroidal fluxes in the northern and the southern hemispheres (see Fig. 2).

Distribution of the radial magnetic field in the final state ($t=5500$) at the outer boundary $B_r(r=r_o)$ viewed from the north is shown in Fig. 7. The view from the south is the same due to the symmetry. The central circle denotes the inner boundary. The six solid thick lines show the loci of cyclonic columns on a spherical plane at $r=0.9$, specifically, the isolines of positive z vorticity ω_z (at the level of 50% of its maximum value). There are six spots of strong B_r flux region (thin contours) whose locations coincide with those of the cyclonic columns. This figure indicates that the magnetic fluxes are accumulated, with equal intensity and polarity, in all the cyclonic columns near the outer boundary. This flux concentration effect is caused by the horizontal converging flow in the cyclonic columns near the outer boundary. The converging flow collects the radial magnetic flux in the cyclonic columns. The flux concentration within the columns is also observed near the equatorial plane and is described in detail in our previous paper [17]. It should be noted that the magnetic flux concentration is observed in the geomagnetic field [34].

E. Toroidal field generation process

We have presented a generation mechanism of the poloidal field in Fig. 5. Understanding of the dynamo mechanism is completed when we present how the toroidal field is converted from the poloidal field. The conversion mechanism is not surprising: It is a well-known ω effect. Figure 8 shows profiles of differential rotation and the convection columns. Thin solid and dashed lines are contours of $\overline{v_\varphi}$ (azimuthally averaged v_φ). The solid (dashed) lines denote eastward (westward) mean flow. The thick solid line shows the contour line of $\omega_z=0.6$ in a meridian cross section which stands for the location of a cyclonic column in this meridian plane. Since the poloidal field is generated in the convection columns, we should focus on the region inside of the thick line in Fig. 8. We can see that there is a westward mean flow in the equatorial plane at the position of the convection columns. The poloidal field lines threading through the equatorial plane from north to south are deformed or drawn by this westward mean flow in the equatorial plane. Therefore, toroidal (east-west) component of the magnetic field is born by this differential rotation; westward in the northern hemisphere and eastward in the southern hemisphere.

The above process of the toroidal field generation by the differential rotation is called the ω effect [15]. An interesting point in this simulation is that the kinetic energy of the differential rotation is only 6% of the total kinetic energy.

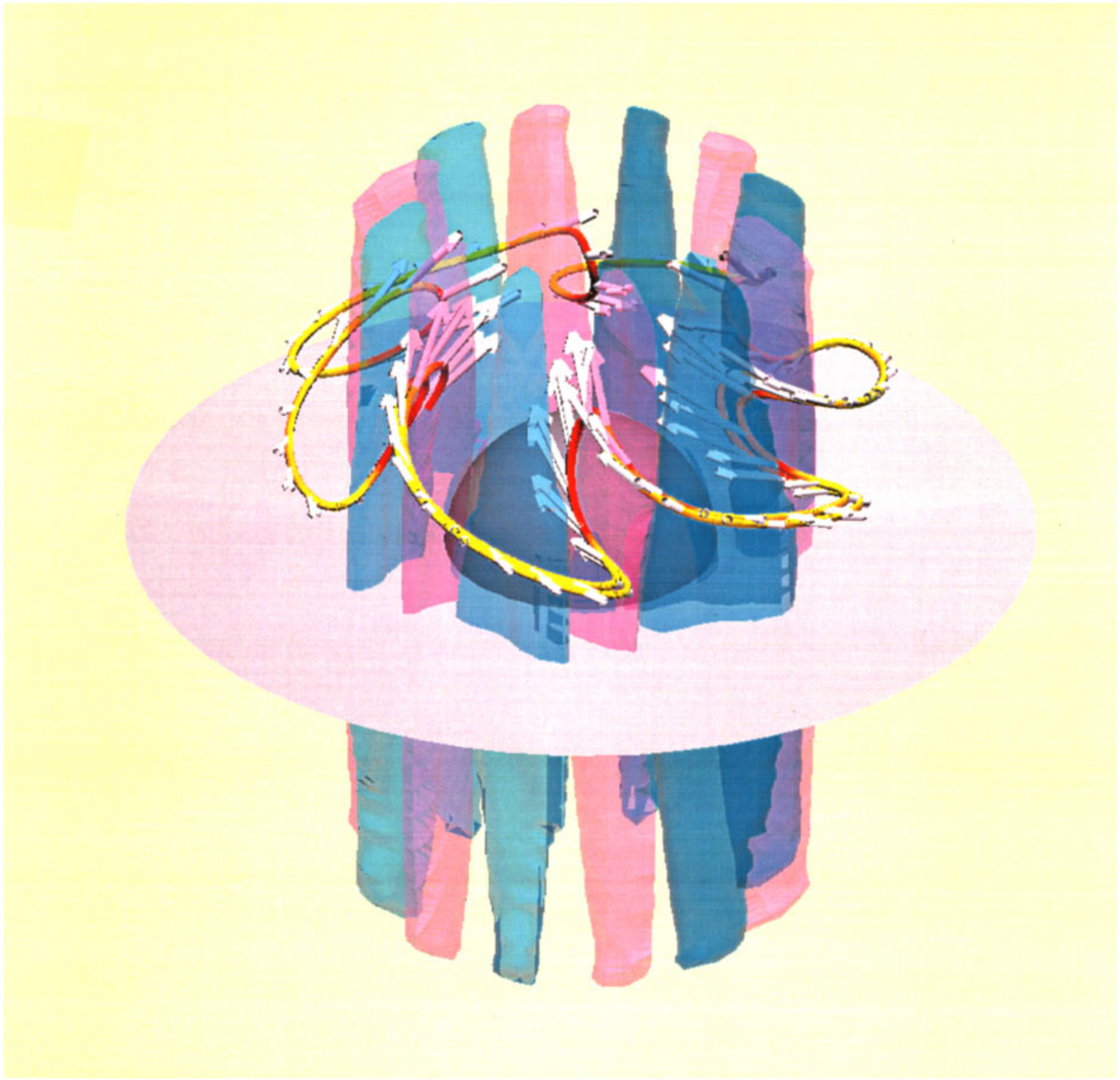

FIG. 6. (Color) A magnetic field line traced at $t=3400$. The line is red where the dynamo term $-\mathbf{v}\cdot\mathbf{J}\times\mathbf{B}$ is large positive. The white arrows denote flow velocity vectors at each point on the line. Blue (pink) semitransparent barlike objects are cyclonic (anticyclonic) convection columns.

Therefore, it should be confirmed that the toroidal field is certainly generated by such a relatively weak differential rotation. For that purpose, we have shown that the magnetic field decays if the differential rotation component is removed from the velocity field. We can take the kinematic dynamo approach in this proof since we are interested only in the magnetic field amplification process, not in the feedback process. In a kinematic dynamo study, time development of the magnetic field is investigated under a fixed velocity field $\mathbf{v}^*$. Here, the velocity $\mathbf{v}^*$ is determined as follows: First, we take the velocity field $\mathbf{v}^o$ from the self-consistent dynamic simulation explained so far in this paper. The data $\mathbf{v}^o$ are taken at $t=256$ when the convection has already reached the saturated state. Then, the axisymmetric component of the longitudinal velocity $\overline{v_\varphi}$, is removed from $\mathbf{v}^o$; $\mathbf{v}^*=\mathbf{v}^o-\overline{v_\varphi}\hat{\varphi}$. From this definition, the velocity field $\mathbf{v}^*$ has exactly no differential rotation. Since $\overline{v_\varphi}$ is weak, the velocity field $\mathbf{v}^*$ is very similar to that of $\mathbf{v}^o$. There are six pairs of cyclonic and anticyclonic convection columns in this case, too. The helical flow pattern in each column, which is the origin of the α effect, is the same as that of $\mathbf{v}^o$. A random weak magnetic field is seeded into this velocity field $\mathbf{v}^*$. Then, it is found that the seed field decays under the fixed velocity $\mathbf{v}^*$. So, there is no dynamo in the absence the differential rotation. For a comparison, the velocity field $\mathbf{v}^*$ is replaced with the original velocity $\mathbf{v}^o$. In this case, the seed magnetic field is amplified. The growing magnetic field has the same

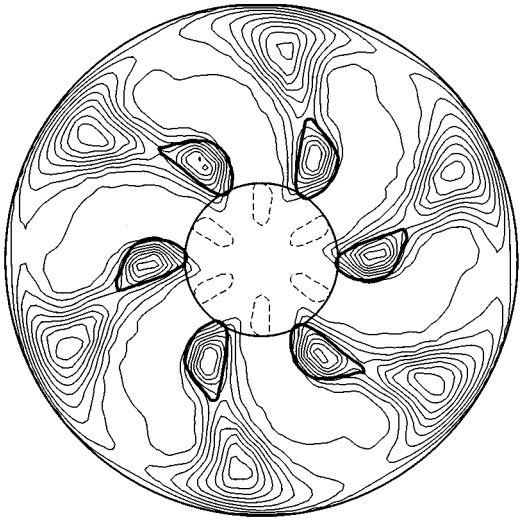

FIG. 7. Distribution of B_r. Contour lines of radial magnetic field B_r at the outer spherical boundary viewed from the north. The central circle denotes the position of the inner spherical boundary. The six thick lines tangent to the inner boundary show the locations of the cyclonic convection columns. One can see that there are six spots of strong B_r flux (thin contour lines). The locations of these spots exactly coincide with those of the cyclonic columns. This flux concentration effect in the cyclonic columns is explained by the converging horizontal flow near the outer boundary in the cyclonic columns. The axial flow in each column, which is downward (upward) in the cyclonic (anticyclonic) columns in this figure, entails horizontal converging flow in the cyclonic columns. The magnetic flux near the outer boundary concentrates by this converging flow in the cyclonic columns.

structure as that of the self-consistent dynamic simulation in its early linear phase before the saturation (Figs. 2 and 3). This is a matter of course since, in the early phase, the growing magnetic is so weak that the $\mathbf{J}\times\mathbf{B}$ force is negligibly small and, therefore, the time development of the magnetic field is essentially kinematic. The above numerical experiments clearly demonstrate that the differential rotation is an indispensable factor for the whole dynamo cycle.

IV. SUMMARY

In summary, we have shown that a dipole magnetic field is spontaneously generated by an MHD thermal convection in a rotating spherical shell. Structure and the generation mechanism of the magnetic field is examined in detail. The poloidal field is generated when toroidal field lines are stretched and deformed by inward flows between cyclonic and anticyclonic convection columns. This process can be understood as an α effect. The generated poloidal field is concentrated in cyclonic convection columns near the outer boundary because of the horizontal convergent flow in the

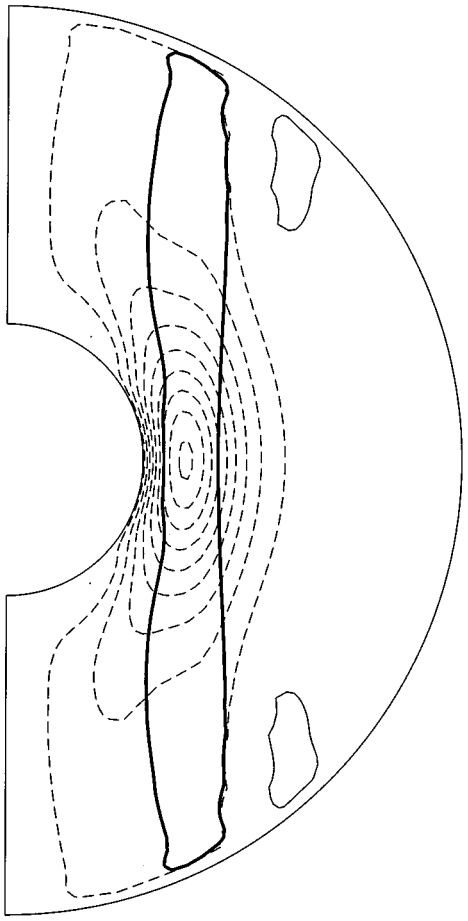

FIG. 8. Differential rotation and the profile of a convection column in a meridian plane. Solid and dashed thin lines are contours of azimuthally averaged velocity of east-west component ($\overline{v_\varphi}$). The dashed lines stand for negative component, i.e., westward mean flow. The thick solid line is a profile of a convection column in a meridian plane cross section. There is a westward mean flow in the equatorial plane at the position of convection columns.

cyclonic columns. Toroidal field is generated from the poloidal field by the westward mean flow in the equator. We can conclude from this simulation that the dipole field generation is a natural consequence arising from the columnar convection structure in the rotating spherical geometry.

ACKNOWLEDGMENTS

The authors would like to thank the Complexity Simulation Group of Theory and Computer Simulation Center, National Institute for Fusion Science for helpful discussions. This work is supported by the Ministry of Education, Science and Culture in Japan.

[1] P.A. Gilman and J. Miller, Astrophys. J. Suppl. **46**, 211 (1981).
[2] P.A. Gilman, Astrophys. J. Suppl. **53**, 243 (1983).
[3] G.A. Glatzmaier, J. Comp. Phys. **55**, 461 (1984).
[4] G.A. Glatzmaier, J. Statistical Phys. **39**, 493 (1985).
[5] G.A. Glatzmaier, Astrophys. Phys. J. **291**, 300 (1985).
[6] G.A. Glatzmaier, Geophys. Astrophys. Fluid Dynamics **31**, 137 (1985).
[7] K.-K. Zhang and F.H. Busse, Geophys. Astrophys. Fluid Dyn. **49**, 97 (1989).
[8] K.-K. Zhang and F.H. Busse, Phys. Earth Planet. Inter. **59**, 208 (1990).

[9] A. Brandenburg, A. Nordlund, P. Pulkkinen, R.F. Stein, and I. Tuominen, Astron. Astrophys. **232**, 277 (1990).
[10] A. Nordlund, A. Brandenburg, R.L. Jennings, M. Rieutord, J. Ruokolanien, R.F. Stein, and I. Tuominen, Astrophys. J. **392**, 647 (1992).
[11] M.G. St. Pierre, in *Theory of Solar and Planetary Dynamos*, edited by M.R.E. Proctor, P.C. Matthews, and A.M. Rucklidge (Cambridge Univ. Press, Cambridge, 1993), pp. 295–302.
[12] G.A. Glatzmaier and P.H. Roberts, Phys. Earth Planet. Inter. **91**, 63 (1995).
[13] G.A. Glatzmaier and P.H. Roberts, Nature **377**, 203 (1995).
[14] E.N. Parker, Astrophys. J. **122**, 293 (1955).
[15] H.K. Moffatt, *Magnetic Field Generation in Electrically Conducting Fluids* (Cambridge University Press, London, 1978).
[16] F. Krause and K.H. Radler, *Mean Field Magnetohydrodynamics and Dynamo Theory* (Pergamon, Oxford, 1980).
[17] A. Kageyama and T. Sato, Phys. Plasmas **2**, 1421 (1995).
[18] A. Kageyama and T. Sato, Research Report NIFS **NIFS-359**, 1995 (unpublished).
[19] A. Kageyama, T. Sato, and K. Watanabe, Phys. Fluids B **5**, 2793 (1993).
[20] M. Stix, *The Sun* (Springer-Verlag, New York, 1991).
[21] *Numerical Recipes in C*, 2nd ed., edited by W.H. Press, S.A. Teukolsky, W.T. Vetterling, and B.P. Flannery (Cambridge University Press, New York, 1992).
[22] P.H. Roberts, Philos. Trans. R. Soc. London Ser., A **263**, 93 (1968).
[23] F.H. Busse, J. Fluid Mech. **44**, 441 (1970).
[24] P.A. Gilman, Solar Phys. **27**, 3 (1972).
[25] G.A. Glatzmaier and P.A. Gilman, Astrophys. J. Suppl. **45**, 351 (1981).
[26] P.A. Gilman and J. Miller, Astrophys. J. Suppl. **61**, 585 (1986).
[27] K.-K. Zhang, J. Fluid Mech. **236**, 535 (1992).
[28] Z.-P. Sun and G. Schubert, Phys. Fluids **7**, 2686 (1995).
[29] S. Chandrasekhar, *Hydrodynamic and Hydromagnetic Stability* (Dover, New York, 1961).
[30] J.B. Taylor, Proc. R. Soc. London A **274**, 274 (1963).
[31] M. Yamada, Y. Ono, A. Hayakawa, M. Katsurai, and F. W. Perkins, Phys. Rev. Lett. **65**, 721 (1990).
[32] Y. Ono, A. Morita, M. Katsurai, and M. Yamada, Phys. Fluids B **5**, 3691 (1993).
[33] T.H. Watanabe, T. Sato, T. Hayashi, and K. Watanabe, J. Plasma Fusion Research **72**, 249 (1996) (in Japanese).
[34] D. Gubbins and J. Bloxham, Nature **325**, 509 (1987).